Paper ID: FM-10

Flow Separation Control on a NACA 0015 airfoil using Plasma Vortex Generator

C. W. Wong*, L. J. Wang, Z. Wu, C. H. Li, Q. Sun, M. M. Alam and Y. Zhou
Institute of Turbulence-Noise-Vibration Interactions and Control, Shenzhen Graduate School
Harbin Institute of Technology, Shenzhen, 518055, China
E-mail: cwwong@hitsz.edu.cn

Abstract

Experimental study has been conducted to determine the effect of plasma vortex generator (PVG) on a NACA 0015 airfoil for flow separation control. The novel design of the PVG consists of an arrangement of two serrated electrodes, with sharp peaks on each electrode facing opposite each other, horizontally separated by a dielectric material. In order to understand the characteristics of the vortex originated from the PVG, measurements including the longitudinal velocity and the spanwise vorticity of the induced flow structure, were conducted in the absence of free airstream using Pitot tube and PIV, respectively. The mechanisms of vorticity generation for PVG are discussed. Lift and drag measurements on the airfoil were conducted at low Reynolds number (7.7×10^4). The PVG showed effective control authority by generating counter-rotating vortices pairs, and it was found to lead to stall delay by 5 degrees and increase in lift coefficient by about 6%.

Keywords: *plasma, vortex generator, flow control*

1. Introduction

In the last decade, application of dielectric barrier discharge (DBD) becomes attractive in the field of flow control from low to moderate Reynolds number *Re* range. DBD plasma actuator is efficient for imparting momentum to the flow much like blowing or suction but without the mass injection. The simplest arrangement of DBD plasma actuator typically consists of a pair of electrodes horizontally separated by dielectric material. An alternating voltage is applied across the electrodes resulting in the generation of plasma in the vicinity of the electrodes. The voltage difference applied between the electrodes can vary from 1 kV to as high as 5 kV, and the frequency of the driving voltage is typically from 1 to 10 kHz [1,2]. The underlying physics, in terms of the plasma morphology and the geometric effects, of DBD plasma actuator was described by Enloe et al. [3,4]. For example, Enloe et al. [4] indicated that the dimensions of the exposed electrode strongly determine the performance of the actuator, and the expansion of the plasma, which is governed in part by the geometry of the lower, insulated electrode, has as considerable an impact on the performance of the actuator as the geometry at the exposed electrode edge. Nevertheless, DBD plasma actuators are commonly studied in asymmetric arrangement such that forcing is produced in longitudinal direction only. Moreau [5] provided comprehensive overview among the worldwide works on the electrical and mechanical characterization of plasma actuators in the absence of free air stream, and the application of plasma actuators for airflow control.

Flow control involves active [6,7,] or passive devices [8,9] with useful end results including lift augmentation, drag reduction, mixing augmentation, and flow-induced noise suppression. The DBD plasma actuators is an important type of active flow control device dedicated to the manipulation of low speed flows [10] and have been successfully applied in numerous flow control applications. These include lift augmentation on a wing section [11], low-pressure turbine blade separation control [12], airfoil flow separation control [13,14], and plasma flaps and slats [15]. In particular, Reference [14] demonstrated that the plasma actuators were found to lead to reattachment for angles of attack that were 8 degrees past the stall angle on a NACA 66_3-018 airfoil section at *Re* ranging from 77×10^3 to 333×10^3. Their experimental results were remarkable, and it showed up to a 400% increase in the lift-to-drag ratio. Reference [15] also indicated that the leading-edge separation control using plasma actuators can achieve the increase of lift-to-drag improvement of as much as 340% at two different *Re* (2.17×10^5 and 3.07×10^5). Recent progress on flow control using DBD plasma actuators can also be found in Reference [16,17].

It is well understood that DBD actuator properties, such as size of the plasma region and generated airflow velocity depend on electrode configuration [4,5,18], dielectric material properties [18,19] and applied voltage [5]. However, other shapes of electrodes, for example, electrode with a serrated edge consisting of triangular patterns in series [18,20-23], were also used to improve airflow and more importantly, to generate the three-dimensional flow topology which could be useful for aerodynamics control applications [23,24]. Joussot et al. [24] demonstrated that the serrated plasma actuator configuration, which had an exposed electrode with a sawtooth edge, generated vorticity between each tip and root, and propagated downstream. However, the transverse velocity levels remain low in comparison with the longitudinal velocity and no well-established counter-rotating vortices were formed. Other geometric shapes of electrodes have also been studied, including the serpentine and square [23, 25], in order to promote a three-dimensional ionic wind. In particular, Wang *et al.* [23] observed the three-dimensional effects such as pinching and spreading the neighboring fluid for serpentine and square actuators. Also, a maximum jet angle at the trough of the square actuator was numerically predicted to be 36 degrees, whereas the jet angle of 35 degrees was experimentally demonstrated for a serpentine actuator.

In this study, the novel design of DBD plasma actuator with sawtooth edge on both exposed and grounded electrodes (plasma vortex generator) is considered, within which the sharp peaks of the serrated electrodes are carefully arranged to facing opposite each other. This serrated design was used in order to induce a three-dimensional ionic wind and more importantly, to increase the vorticity in the same way as yawed DBD actuators dedicated for flow separation control by vortex generation [26]. Firstly, the plasma vortex generator has been characterized by the measurements of longitudinal velocity and spanwise vorticity of the flow structure in the absence of free air stream using Pitot tube and particle image velocimetry, respectively. Secondly, we demonstrate the effect of a spanwise-oriented plasma vortex generator on a NACA 0015 airfoil based on force measurement from which we could determine the improved stall angle and lift coefficient. Details of the plasma vortex generator PVG and the experimental setup are summarized in Sec. 2. The results showing time-averaged velocity profiles, streamwise vorticity generated by the PVG, and the lift and drag coefficients of the airfoil are discussed in Sec. 3. Finally, conclusions and future works are drawn in Sec. 4.

2. Experimental Details

2.1 Actuator Design

The design of DBD plasma actuator has a sawtooth edge on both exposed and grounded electrodes, and is called the plasma vortex generator (PVG) in this study. The PVG consists of two metallic electrodes made out of adhesive copper foil tape separated by a thin PMMA material of 1 mm thickness. In order to investigate the characteristics of the ionic wind and the streamwise vortical structures originated from the PVG, a prototype of PVG has six sawtooth distributed uniformly along an edge of each serrated electrode is constructed (Fig. 1). The height h and width w of each sawtooth is 1.5 mm and 17.0 mm, respectively. The overall dimension of each exposed and grounded electrode is 140 mm in length, 15 mm wide, and 0.15 mm thick. The exposed electrode is connected to an AC power supply, that the output voltage is controlled by a signal generator (Rigol DG 4062). Thus, it could deliver sine voltage V_p of 8–20 kV in amplitude with a frequency of about 5000–15000 Hz. The grounded electrode is connected to the earth terminal of the AC power supply, and is encapsulated with an insulating tape to avoid plasma formation on this side. The electrical parameters are visualized with an oscilloscope (Rigol DS2072). The voltage is measured with a high voltage probe (Tektronix P6015A), whereas the current is measured by using a current probe (Tektronix P6021) in series with the discharge setup, placed between the ground and the grounded electrode (Fig. 2).

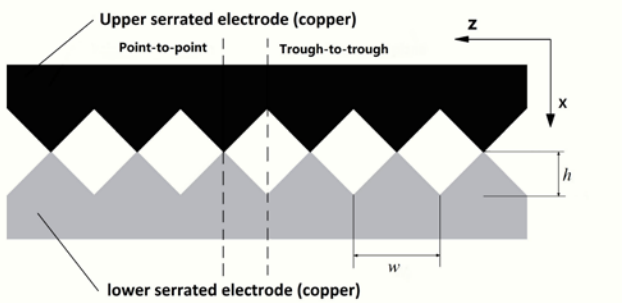

Fig. 1. Illustration of the prototype of plasma vortex generator

2.2 Characterization of the PVG

Firstly, the flow generated by the PVG is measured by using a Pitot tube, giving a time-averaged velocity of the ionic wind. The Pitot tube is a glass tube having an inner diameter of 0.5 mm, which resulting an accuracy of

a few μm in x- and y- directions. The glass tube is connected to a Furness FCO510 micromanometer (0–20 mmH_2O, 0–18 m/s) by a Tygon tube of about 0.5 m long. The glass tube can be travelled along 3 axes above the actuator with the three-component traverse, which has 0.02 mm displacement accuracy, controlled by a computer. The analog output of the micromanometer is connected to the FCS487 Data logger. For each measure, 450 samples at 5 Hz are recorded in order to seek the convergence of the time-averaged velocity value.

Secondly, the induced vorticity is examined by using the particle image velocimetry (PIV). The PVG is operated in a quiescent environment in an Acrylic glass box (500 mm length × 500 mm width × 800 mm height), which is seeded using a TSI 9307-6 particles generator. The particle droplets are on average 1 μm in diameter, and are generated from olive oil. The PIV system consists of a dual beam laser system (Litron LDY304-PIV, Nd: YLF), a CCD camera and a PC. A laser sheet of about 2 mm thickness is formed above the PVG. The time between pulses is 150 μs, and the trigger rate is 727 Hz for double frame mode. The PIV data presented in this paper are the average of 200 image pairs within which 200 vector fields are recorded. The images are recorded using a Vision Research high-speed camera (Phantom V641) with a 4-megapixel sensors and 2560 pixels × 1600 pixels resolution. The viewing area used for the calculations of the vector fields is 102 mm × 37 mm. Post-processing of the velocity data is conducted using Tecplot. Figure 2 shows the schematic of experimental setup for the PIV measurements.

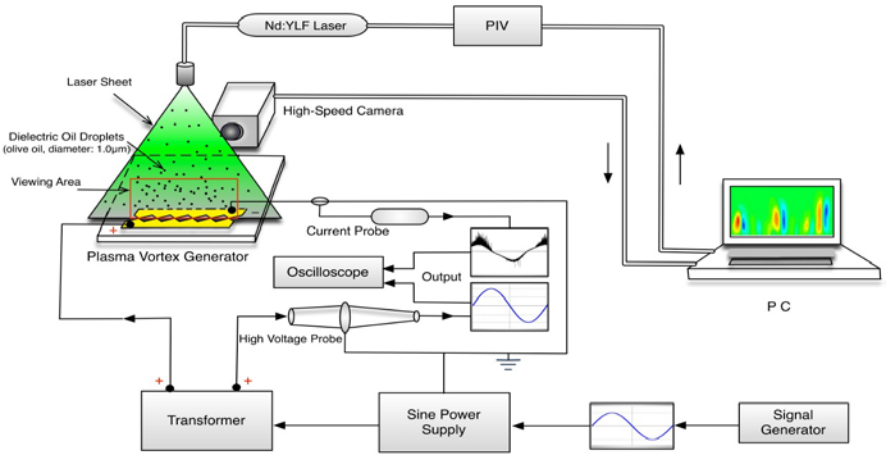

Fig. 2. Schematic of experimental setup for the PIV measurements

2.3 Force Measurement

Force measurements were performed in a closed circuit wind tunnel with a working section of $L \times W \times H$ = 3.0 m × 0.8 m × 1.0 m. The non-uniformity of the flow in the test section was no more than 0.5% and the free-stream longitudinal turbulence intensity was approximately 0.4% for the *Re* examined. The freestream velocity was measured using a Pitot–static tube connected to a Furness micromanometer, with an uncertainty of less than 2.0%. A NACA 0015 airfoil model with the span of 300 mm and the chord length of 200 mm was investigated at a freestream velocity U_∞ of 6 m/s, which results in chord *Re* of 7.7×10^4. No boundary-layer trips were employed. The PVG consisting of 10 pairs of sharp peaks, covering the central 60% of airfoil span, was installed at 2% downstream from the leading-edge and on the suction side of the airfoil. The airfoil model was vertically suspended between two false walls in the test section, and the lift and drag forces were measured using a three component load cell (LSM-B-SA1, 10 N). The load cell has a rated output of 0.5 mV/V, and the hysteresis is ±0.5%. The time-averaged aerodynamic forces were measured with a moderate sampling rate of 1.0 kHz, and a 500 Hz filter was used in the data acquisition system. The accuracy of the lift and drag measurements is approximately ±0.05%. Aerodynamic forces were normalized by the freestream dynamic pressure and airfoil area. Note that the angle of attack α of the airfoil section is set by a rotary table, and the uncertainty on the angle of attack is approximately 0.25.

3. Results and Discussions

The time-averaged velocity profile [Figs. 3(a) and (b)] were recorded at the peak-to-peak location (Fig. 1) and along the *X*-*Y* plane. Figure 3(a) shows the corresponding velocity profile, captured using Pitot tube, for a given *X* position. At a voltage V_p of 11 kV and frequency *f* of 11 kHz, the maximum velocity of about 2.64 m/s is obtained at X = 5 mm and Y = 0.3 mm. Indeed, each maximum velocity is found close to the wall with *Y* ranging from 0.3 to 0.7 mm. The velocity gradually decreases with increasing *Y* due to the momentum diffusion from the plasma to the surrounding air. It is noteworthy that the momentum delivered to the surrounding air by the charged species at the peak-to-peak location is much greater than that of the trough-to-trough location, thus,

resulting an approximately two-dimensional induced flow in the *X*-*Y* plane. The effect of the applied voltage is investigated and presented in Fig. 3(b). It can be seen that the velocity increases from 0.96 to 3.33 m/s with the applied voltage ranging from 11 to 15 kV.

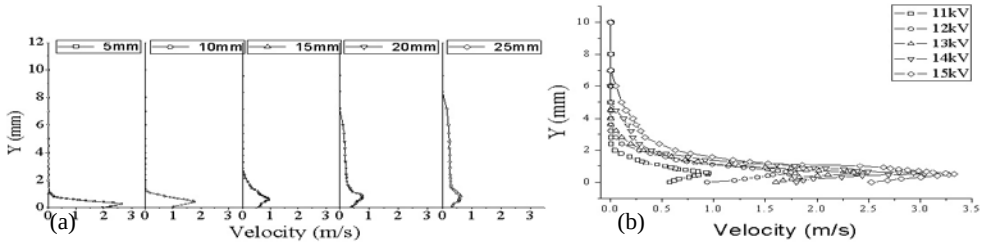

Fig. 3. (a) Velocity profiles at different *X* positions (f = 11 kHz, V_p = 11 kV); (b) Velocity profiles for different voltage amplitudes, at X = 15 mm (f = 11 kHz)

The PIV tests were conducted to observe the evolution of the vortex structures that originated from the PVG upon actuation. Figure 4 shows that the streamwise vortices are uniformly generated in *Z* direction. This is due to the serrated electrodes which locally varied the electric field, that vortices are generated on either side of each sharp peak. Based on the cross–correlation analysis, the maxima of ω_x of about ±6201 s^{-1} (not shown) was achieved at X = 15 mm. The presently identified streamwise vortices do not collide together, which differs from Refs. [21] and [24], thus avoiding substantial interactions between vortices, and the vortices could persist longer in the downstream locations. One can observe that the vortices lift away from the wall at *X* between 30 and 50 mm. This is attributed to the vortices from one pair begin to interact with the vortices from adjacent pairs, thus creating common-flow up configurations as seen in at X = 50 mm (Fig. 4).

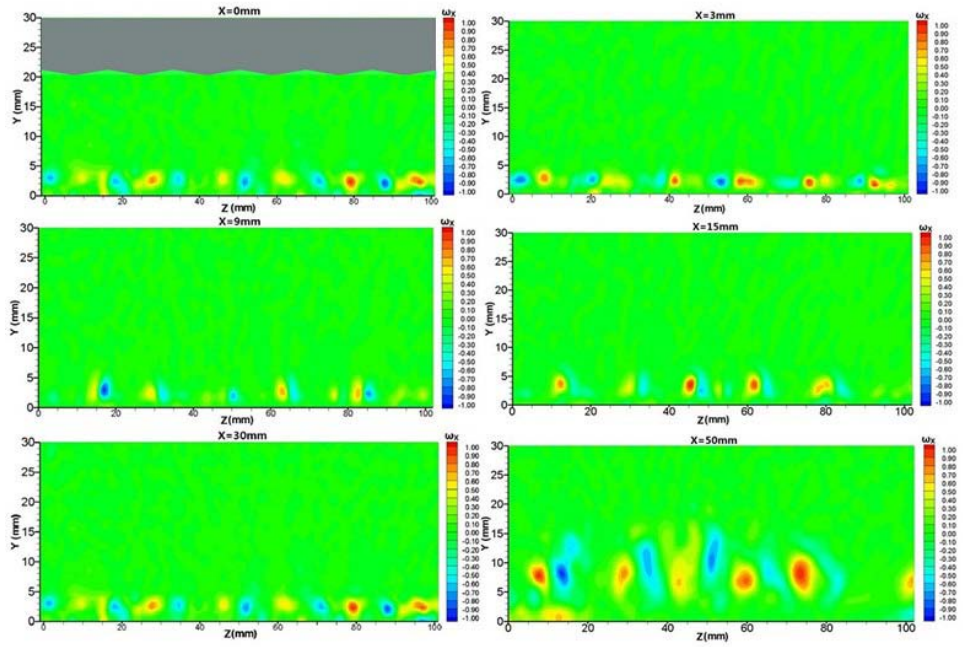

Fig. 4. Vorticity contours in the spanwise direction at different X positions (f = 11 kHz, V_p = 11 kV, X = 0, 3, 9, 15, 30 and 50 mm)

Due to the unique electric field between the serrated electrodes, the interaction exists between the streamwise vortices ejected out near the sharp peak of the electrode and the flow structure at the sharp peak location, thus forming small vortices close to the wall at the peak [Fig 5(a)]. On the other hand, the directed vortices at the trough show a maximum inducement angle of about 26^o [Fig 5(b)]. One can observe clearly that the trains of vortices close to the wall, from X = 20 mm to 70 mm, are due to the Kelvin–Helmholtz (*K*-*H*) instability

generated by the directed vortices. It should be noted that the strength of the *K-H* instability is in an order similar, but opposite, to that of the directed vortices.

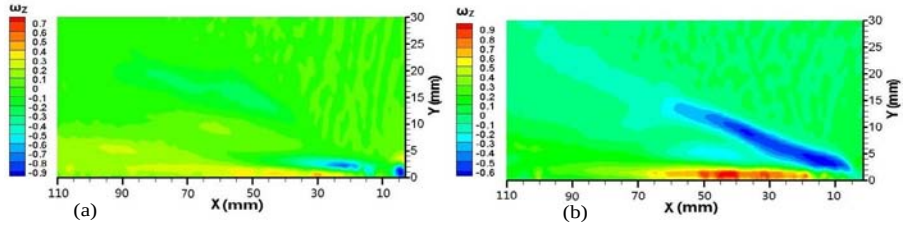

Fig. 5. Vorticity contours in the longitudinal direction (f = 11 kHz, V_p = 11 kV); (a) at the tip location; (b) at the trough location

The effect of the plasma vortex generator is shown in Fig. 6, in which lift and drag coefficients of the airfoil with actuation (i.e. V_p varies between 11 and 15 kV) are compared with those of the baseline airfoil (i.e. applied voltage V_p is zero). It is noteworthy that the slope in the lift drop determines the flow regime as discussed in Ref. [27], and by the reason thereof, the naturally developed boundary layer on the suction side of the NACA 0015 airfoil (i.e. baseline, V_p = 0) progresses from laminar to local separation then to turbulent reattachment (i.e. the laminar separation bubble) and finally to turbulent separation as confirmed by the lift coefficient C_l vs. angle-of-attack α curve in Fig. 6(a). It is evident that the PVG has a beneficial effect on the lift coefficient (Fig. 6a). The data indicated that the spanwise-orientated PVG along the span of the airfoil improves the lifting performance, reflected in the delay of stall angle and increase in the maximum lift coefficient of about 5 degrees and 6%, respectively. This is attributed to the mixing of high-momentum freestream fluid, induced by the counter-rotating vortex pairs, takes place toward the near wall region, and thus reattaches the flow. The C_l-α curve for the case of V_p = 15 kV demonstrates that the boundary layer changes from laminar to transition to turbulent, then separates at α = 18 degrees. Note that the decrease in drag coefficient is significant for the case of V_p = 15 kV as revealed in Fig. 6(b). The result also suggests only small considerable benefits could be achieved at α less than the stall angle for V_p is between 11 kV and 13 kV. The cause of this could be related to the elimination of laminar separation bubble caused by the induced counter-rotating vortex pairs of the PVG, and as a result, the drag coefficient is reduced accordingly (Fig. 6b).

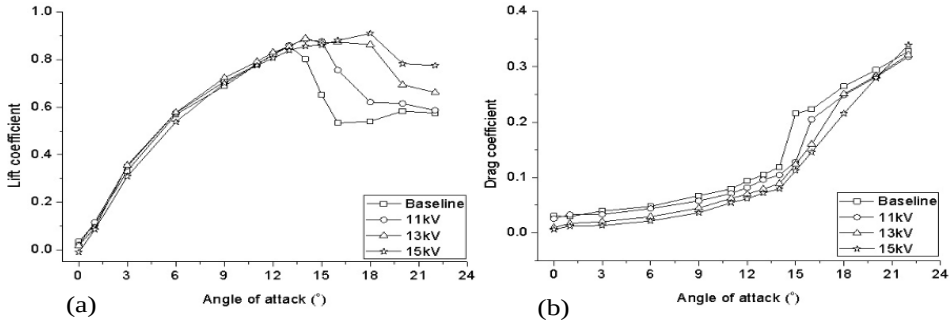

Fig. 6. (a) Lift coefficient versus angle-of-attack (V_p ranging from 11 to 15 kV); (b) Drag coefficient versus angle-of-attack (V_p ranging from 11 to 15 kV)

4. Conclusions

This paper focused on the study of plasma vortex generator PVG, which consists of two serrated electrodes, with the sharp peaks on each electrode facing opposite each other, and horizontally separated by a dielectric material, as well, the aerodynamics effect of a NACA 0015 airfoil with actuation and at $Re = 7.7 \times 10^4$.

In the absence of a free air stream, it can be clearly seen that the counter-rotating vortices are uniformly created in the spanwise direction. In addition, the streamwise vortices do not collide together, thus avoiding substantial interactions between vortices, and the vortices could persist longer in the downstream locations.

The results from the force measurements indicate that the spanwise-oriented plasma vortex generator brings high momentum fluid into the wall region in such a way that the maximum lift coefficient was increased by about 6%, while, at the same time, the stall angle was postponed from 13 to 18 degrees. Further experiments will be carried out in order to examine the flow structure of streamwise vortices and vortex pairs on the suction

side of the airfoil, which may be useful to improve the PVG design for flow separation control.

5. Acknowledgement

This work was supported by Natural Scientific Research Innovation Foundation in Harbin Institute of Technology (Grant No. HIT.NSRIF.2013098), and Shenzhen Government (Grant No. JC201105160543A).

6. References

[1] G.I. Font, "Boundary Layer Control with Atmospheric Plasma Discharges", *AIAA Journal*, Vol. 44, No. 7, pp. 1572-1578, 2006.
[2] T.N. Jukes, K.S. Choi, G.A. Johnson, and S.J. Scott, "Characterization of Surface Plasma-Induced Wall Flows Through Velocity and Temperature Measurements", *AIAA Journal*, Vol. 44, No. 4, pp. 764-771, 2006.
[3] C.L. Enloe, T.E. McLaughlin, R.D. VanDyken, K.D. Kachner, E.J. Jumper, and T.C. Corke, "Mechanisms and Responses of a Single Dielectric Barrier Plasma Actuator: Plasma Morphology", *AIAA Journal*, Vol. 42, No. 3, pp. 589–594, 2004a
[4] C.L. Enloe, T.E. McLaughlin, R.D. VanDyken, K.D. Kachner, E.J. Jumper, and T.C. Corke, "Mechanisms and Responses of a Single Dielectric Barrier Plasma Actuator: Geometric Effects", *AIAA Journal*, Vol. 42, No. 3, pp. 595–605, 2004b.
[5] E. Moreau, "Airflow Control by Non-thermal Plasma Actuators", *Journal of Physics D: Applied Physics*, Vol. 40, No. 3, pp. 605–636, 2007.
[6] C. Wong, and K. Kontis, "Flow Control by Spanwise Blowing on a NACA 0012", *Journal of Aircraft*, Vol. 44, No. 1, pp. 337-340, 2007.
[7] C. Wong, and K. Kontis, "Pneumatic Flow Control Studies Using Steady Blowing on a Supercritical Aerofoil", *The Aeronautical Journal*, Vol. 113, No. 139, pp. 53-63, 2009.
[8] M.B. Bragg, and G.M. Gregorek, "Experimental Study of Airfoil Performance with Vortex Generators", *Journal of Aircraft*, Vol. 24, No. 5, pp. 305–312, 1987.
[9] K. Rinoie, M. Okuno, and Y. Sunada, "Airfoil Stall Suppression by Use of a Bubble Burst Control Plate", *AIAA Journal*, Vol. 47, No. 2, pp. 322–330, 2009.
[10] J.R. Roth, D.M. Sherman, and S.P. Wilkinson, "Boundary Layer Flow Control with a One Atmosphere Uniform Glow Discharge Surface Plasma", AIAA Paper 98-0328, 1998.
[11] T. Corke, E. Jumper, M.L. Post, D. Orlov, and T. McLaughlin, "Application of Weakly-Ionized Plasmas as Wing Flow-Control Devices", AIAA Paper 02-0350, 2002.
[12] J. Huang, T. Corke, and F. Thomas, "Plasma Actuators for Separation Control of Low Pressure Turbine Blades," AIAA Paper 03-1027, 2003.
[13] M.L. Post, and T. Corke, "Separation Control on High Angle of Attack Airfoil Using Plasma Actuators," *AIAA Journal*, Vol. 42, No. 11, pp. 2177–2184, 2004.
[14] B. Goeksel, I. Rechenberg, D. Greenblatt, and C.O. Paschereit, "Steady and Unsteady Plasma Wall Jets for Separation and Circulation Control," AIAA Paper 06-3686, 2006.
[15] H. Chuan, T.C. Corke, and M.P. Patel, "Plasma Flaps and Slats: An Application of Weakly Ionized Plasma Actuators", *Journal of Aircraft*, Vol. 46, No. 3, pp. 864-873, 2009.
[16] T.C. Corke, M.L. Post, and D.M. Orlov, "SDBD Plasma Enhanced Aerodynamics: Concepts, Optimization and Applications", *Progress in Aerospace Sciences*, Vol. 43, Nos. 7–8, pp. 193–217, 2007.
[17] T.C. Corke, C.L. Enloe, and S.P. Wilkinson, "Dielectric Barrier Discharge Plasma Actuators for Flow Control," *Annual Review of Fluid Mechanics*, Vol. 42, pp. 505-529, 2010.
[18] F.O. Thomas, T.C. Corke, M. Iqbal, A. Kozlov, and D. Schatzman, "Optimization of Dielectric Barrier Discharge Plasma Actuators for Active Aerodynamic Flow Control", *AIAA Journal*, Vol. 47, No. 9, pp. 2169–2178, 2009.
[19] M. Forte, J. Jolibois, J. Pons, E. Moreau, G. Touchard, and M. Cazalens, "Optimization of a Dielectric Barrier Discharge Actuator by Stationary and Non-Stationary Measurements of the Induced Flow Velocity: Application to Airflow Control", *Experiments in Fluids*, Vol. 43, No. 6, pp. 917–928, 2007.
[20] A. Berendt, J. Podli´nski, and J. Mizeraczyk, "Comparison of Airflow Patterns produced by DBD Actuators with Smooth or Saw-Like Discharge Electrode", *Journal of Physics: Conference Series*, Vol. 301, 012018, 2011.
[21] Z. Liu, L. Wang, and S. Fu, "Study of Flow Induced by Sine Wave and Saw Tooth Plasma Actuators", *Science China: Physics, Mechanics and Astronomy*, Vol. 54, No. 11, pp. 2033–2039, 2011.
[22] N. Balcon, N. Benard, Y. Lagmich, J.P. Boeuf, G. Touchard, and E. Moreau, "Positive and Negative Sawtooth Signals applied to a DBD Plasma Actuator - Influence on the Electric Wind", *Journal of Electrostatics*, Vol. 67, No. 2-3, pp. 140–145, 2009.
[23] C.C. Wang, R. Durscher, and S. Roy, "Three-Dimensional Effects of Curved Plasma Actuators in Quiescent Air", *Journal of Applied Physics*, Vol. 109**,** 083305, 2011.
[24] R. Joussot, A. Leroy, R. Weber, H. Rabat, S. Loyer and D. Hong, "Plasma Morphology and Induced Airflow Characterization of a DBD Actuator with Serrated Electrode" *Journal of Physics D: Applied Physics*, Vol .46, 125204, 2013.
[25] R. Durscher, and S. Roy S, "Three-Dimensional Flow Measurements Induced from Serpentine Plasma Actuators in Quiescent Air", *Journal of Physics D: Applied Physics*, Vol. 45, 035202, 2012.
[26] T.N. Jukes, and K.S. Choi, "Dielectric-Barrier-Discharge Vortex Generators: Characterisation and Optimisation for Flow Separation Control, *Experiments in Fluids*, Vol. 52, pp. 329-345, 2012.
[27] M.P. Patel, Z.H. Sowle, T.C. Corke, and C. He, "Autonomous Sensing and Control of Wing Stall using a Smart Plasma Slat", *Journal of Aircraft*, Vol. 44, No. 2, pp. 516–527, 2007.